Global Advanced Research Journal of Agricultural Science (ISSN: 2315-5094) Vol. 5(1) pp. 051-060, January, 2016 Issue.
Available online http://garj.org/garjas/home

Full Length Research Papers

Detection of Sea Surface Temperature and Thermal Pollution of Agricultural Coastal Areas using Thermal Infrared, Jeddah City, West KSA

Amal Yahya Alshaikh

King Abdul Aziz University, Jeddah,Saudi Arabia
Email: sh99amal@gmail.com

Accepted 31 January, 2016

Thermal pollution of marine water adversely affects the local environment and ecosystems due to consequent rise in water temperature. Industrial activity, particularly cooling process, is the main reason of marine pollution. The current study is focusing on thermal coastal water pollution in Jeddah city (west KSA). It is aimed to estimate water temperature using satellite data, particularly thermal bands. Temporal and spatial variation, of sea surface temperature (SST) are followed using Landsat 5 Thematic Mapper (TM) scenes, and Landsat7 Enhanced Thematic Mapper (ETM), acquired in (September 1990), (October 2000) and (November 2013). Thermal infrared (TIR) remote sensing data were used to calculate Sea Surface Temperature (SST). It was found that the highest SST value, recorded within the period 1990-2000, was (29°C), whereas the highest (SST) in the year 2013 jumped to be 33°C. The lowest (SST) found within year 1990-2000 is (26°C), while (29°C) was found in year 2013. The increase of SST, during 1990-2013, is an evidence of thermal pollution occurring along Jeddah city coastal area. It is expected that such pollution has its impact on local aquatic organisms status and activates (i.e. metabolic rates, reduction of cell wall permeability, osmotic pressure, enzyme systems … etc.).

Keywords: Sea Surface Temperature (SST), Thermal Infrared (TIR), Thermal Pollution, Jeddah City

INTRODUCTION

Transgression on marine habitats (seagrass beds, coral reefs and mangrove stands) along the Jeddah coast and adjacent lagoons, owing to increased human activity, resulted in regression, on degeneration or substitution of plant and animal communities. The effect of organic and thermal pollution on benthic life is examined. A need for baseline studies on such habitats is stressed for the identification and conservation of endangered biota (Aleem, 1990). Coastal thermal pollution is a change in the physical, chemical and biological characteristics of water & sediments, causes degradation of the natural quality of the coastal environments, and affects the health and survival of all life forms. Such pollution represents a major problem in developing countries, moreover trends are expected to increase (Sarkar et. al. 2008). One of the major causes of thermal pollution is the industrial use of water as a coolant.

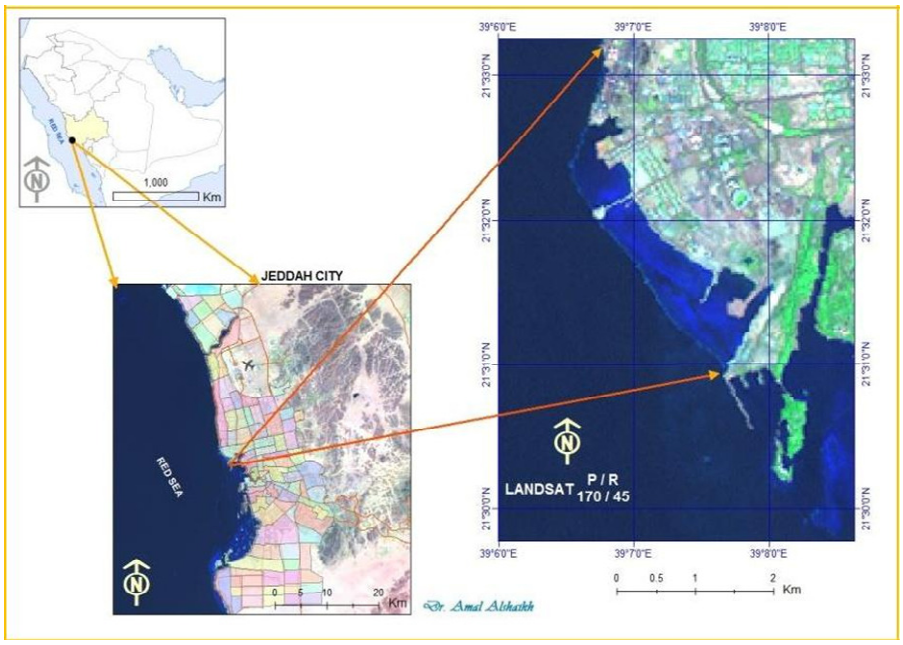

Figure 1: Location map of study area

Table 1: Satellite images used in the study area

Dateacquired	Data_Type	Spacecraft_ID	SENSOR_ID	PATH/ROW	Resolution band 6	Wavelength(µm)
11-09-1990	LT5	LANDSAT_5	TM	170/ 45	60m	10.40 - 12.50
01-11-2000	LE7	LANDSAT_7	ETM	170/ 45	30m	10.40 - 12.50
04-10-2013	LE7	LANDSAT_7	ETM	170/ 45	30m	10.40 - 12.50

Factories and power plants typically use nearby water sources to keep machinery cool and functional. While inexpensive and effective, this form of cooling process can wreak havoc on aquatic ecosystems. Water is typically siphoned away from a source, run through cooling systems at a factory or plant, and then returned to the original source Thermal Infrared (TIR) (WiseGEEK, 2014). Coastal industries in the Red Sea region include power and desalination plants, refineries, fertilizer manufacturers and chemical plants. At present these industries and their effluents (oil, organic pollutants, heavy metals, heated brine and cooling water) are consideredimportant problems in every country of the region (Persga , 1997). Grave Thermal pollution of the sea involves serious risks for cities and coastal marine ecosystems, also constitutes the main threat to marine life, as they can infect and kill marine organisms (animals and plants), including Coral reefs, Fish and Mangroves. The resulting impact on the marine ecosystems due to thermal pollution and the elevated levels of salt and chlorine in the return waters vary with the volumes of water and the location of the discharge. Discharges into the marine environment from the Jeddah plants include chlorine and anti-sealant chemicals as well as brine which exceeds by 1.3 times the ambient salinity of the Red Sea (Persga , 1997). Thermal Infrared Remote sensing (TIR) is a branch of remote sensing dealing with IR waves (Prakash, 2000). It can provide important measurements of surface energy fluxes and temperatures, which are integral to understand landscape processes and responses (Quattrochi and Luvall 1999) . TIR measurements can be used for observing water temperature (Carbonneau and Piégay 2012). It can significantly contribute to the observation, measurement, and analyses of energy balance characteristics (i.e., the fluxes and redistribution of thermal energy within and across the land surface) as an implicit and important aspect of landscape dynamics and landscape functioning (Quattrochi and Luvall 1999) (Quattrochi and Luvall 1999). Remote sensing data are acquired in predetermined spectral bands (wave lengths). Visible and near infrared spectral bands (which can be displayed in colors as shown in Figure (1) are chosen to amplify or separate specific earth features such as vegetation, rocks, urban area, snow and water. This way one can separate a chosen land

feature from other land features by choice of the wavelength (Simonovic and Eng, 2002). Thermal remote sensing is based on recording the electromagnetic radiation in the thermal infrared region (TIR) emitted by surface objects as a function of their temperature in two windows: 3.5–5 µm and 8.0–14.0 µm. Therefore, thermal images can be acquired during both day and night (UNESCO, 2007). Thermal infrared remote sensing (TIR) technique is a useful approach to monitor change of water temperature (UNESCO , 1982). TIR Bands of Landsat-5 Thematic Mapper (TM), Landsat-7 Enhanced Thematic Mapper (ETM) has wide range of electromagnetic wavelength band, including visible, infrared and thermal bands. Its thermal bands can detect thermal radiation released from objects on the earth surface (Xing and Chen, 2006). TIR data can aid identifying a severe environmental phenomenon: thermal pollution resulting from power planet and industry discharges of water used in cooling processes. Aquatic life gets affected as the seemingly harmless thermal pollution lowers dissolved oxygen and increases respiration rates, killing an ever increasing quantity of fish in their positive feedback cycle. The density and viscosity of water also decrease as temperature increases. This results in a faster settling of suspended solids. The rate of evaporation significantly increases too as temperature increases, resulting in a greater wastage of water in the form of its vapor (Tarntino and Aiello, 2011).

STUDY AREA

Jeddah city is located in west of KSA, Extents between (21°30'00"–21°33'00")N and (39°06'00"- 39°08'00")E (Figure 1). Jeddah population is (3.4 millions).

Jeddah is located in Saudi Arabia's Red Sea coastal plain (called Tihamah). It lies in the Hijazi Tihama region which is located in the lower Hijaz mountains. Historically, politically and culturally, Jeddah was a major city of Hejaz Vilayet, the Kingdom of Hejaz and other regional political entities according to Hijazi history books. It is the 100th largest city in the world by land area. Jeddah features an arid climate (*BWh*) under Koppen's climate classification. Unlike other Saudi Arabian cities, Jeddah retains its warm temperature in winter, which may range from 15 °C (59 °F) at dawn to 28 °C (82 °F) in the afternoon. Summer temperatures are extremely hot, often breaking the 43 °C (109 °F) mark in the afternoon and dropping to 30 °C (86 °F) in the evening. Rainfall in Jeddah is generally sparse, and usually occurs in small amounts in November and December. Heavy thunderstorms are common in winter. The thunderstorm of December 2008 was the largest in recent memory.

METHODOLOGY

Remote Sensing and GIS are powerful tools which provide solutions for water resources management problems. They may serve the assessment of water quality and water availability and flood problems, management. Remote sensing multi-concept helps understanding the natural environment, and managing water resources on local and regional levels (Stefouli et.al. 2013).

This study used the thermal infrared (TIR) remote sensing, from the satellite images of Landsat Thematic Mapper (TM) scenes from Landsat 5, and the Landsat Enhanced Thematic Mapper (ETM) of Landsat7. The data were Acquired in (September 1990), (October 2000) and (November 2013). The study area is covered by scene identified (path/row) 170/45 (Table1).

The analyses were carried out according to the algorithm of convert the DN of thermal band of Landsat 5 (TM) and 7 (ETM+) data to radiance, reflectance values and then converted to blackbody temperature. The obtained values are used in calculating the surface albedo, emissivity, and transmissivity as adjustment parameters to convert the blackbody temperature to surface temperature as shown in the following steps.

Determining Area of Thermal Pollution

Beginning, by Visual interpretation may allow identifying areas of thermal pollution on the Landsat imagery. ENVI software was used to get the FCC imagery by assigning the bands to RGB filters, as bands composite (B6, B2, B1). Then, the highlighted pixels refer to the area ofthermal pollution. By using ERDAS Imagine software in this study, thermal bands of TM and ETM) sensors were used to compute SST. In order to detect changes occurring in SST, multi temporal data were utilized. A number of 10 selected thermal polluted locations for each year image (band 61 in 1990, band 62 in 2000, band 62 in 2013) were assessed.

Retrieve Sea Surface Temperature (SST)

Satellite imagery is commonly stored in Digital Numbers (DN) for minimizing the storage volume, i.e. the originally sampled analog physical value (color, temperature, etc.) is stored a discrete representation in 8-16 bits. For example, Landsat data are stored in 8bit values (i.e., ranging from 0 to 255) (Mitasova and Neteler, 2004).

This study used 3 set of Landsat-5 TM and Landsat-7 ETM data AVHRR data for September, October, and November as shown in Table 1. Following the geometric and radiometric correction preprocessing, convert the digital number (DN) values (ranging from 0 to 255) in Landsat thermal band (band 61 and band 62) to spectral radiance value, and then to blackbody (TOA) temperature value. Also convert the DN to reflectance values to be used in calculation of surface albedo and transmissivity. The last step is to use the surface albedo and transmissivity values to convert the blackbody temperature to land surface temperature as indicated in Figure (2):

Step.1. Data collection and processing: It started with geometric correction and thenradiometric correction. The

Table 2: Measurements of digital number (DN) at selected locations from study area

Lat	Long	DN–1990	DN–2000	DN–2013
21°32'39.7931"N	39°6'50.2871"E	150	175	185
21 32 37.1993 N	39 6 49.1432 E	149	173	183
21 32 32.0155 N	39 6 41.3088 E	149	172	181
21 32 30.1868 N	39 6 37.0660 E	148	172	181
21 32 27.5975 N	39 6 29.0706 E	143	165	178
21 32 14.1595 N	39 6 40.1533 E	147	170	179
21 32 25.2441 N	39 6 44.9776 E	148	171	190
21 32 10.0256 N	39 6 35.9668 E	146	167	177
21 32 10.2569 N	39 6 34.9807 E	145	162	176
21 32 25.815 N	39 6 27.661 E	142	163	175

Table 3: (DN) (gain & bias) values in landsat5-TM

landsat5-TM	P / R	Gain	Bias
11/09/1990	170 / 45	0.055158	1.237800

Table 4: (Lmax - Lmin) values in landsat7-ETM

Parameters	Lmin	Lmax
Landsat-7 ETM-B62- P/R-170/45 (01/11/2000 & 04/10/2013)	3.200	12.65

digital number (DN) value in thermal bands (band 61 and band 62)were converted to spectral radiance (L) values, using any two methods depending on the scene calibration data available in the header file.

Gain and Bias Method (Irons, 2012)**.**

$$CV_R = G\,(CV_{DN}) + B \qquad (1)$$

Where:

CV_R is the cell value as radiance, CV_{DN} is the cell value digital number,G is the gain value for a specific band in watts/ (meter squared *ster * µm), B is the bias value for a specific band in watts/(meter squared * ster * µm).

Table (4) lists (gain & bias) values for landsat5-TM band 6.

LMin and LMax Method: (Irons, 2012).

$$L = ((LMAX - LMIN)/ (DNMAX-DNMIN))* (DN-DNMIN) +LMIN \quad (2)$$

Where:

L = Spectral radiance watts/(m*m * ster * µm) DN= Digital Number

LMIN= Spectral radiance which is correlate with DNMIN MAX= Spectral radiance which is correlate with DNMAX

DNMIN=Minimum value of DN (1 (LPGS Product) or 0 (NLAPS Product)) DNMAX=Maximum value of DN = 255

Table4 lists these values for landsat7- ETM band 62.

Step.2. Conversion of spectral radiance to temperature in Kelvin (Irons, 2012)**.**

$$T = K2/ (\ln(k1/L)+1) \quad (3)$$

Where:

T= Effective at-satellite temperature in Kelvin

K2= Calibration constant 2 from Table 4

K1= Calibration constant 1 from Table 4

L= Spectral radiance in watts/ (meter squared * ster * µm)

"Landsat 7 ETM Thermal Band Calibration Constants are listed in table (5). To convert the at-satellite temperature to land surface temperature, many parameters are need to calculated i.e. surface albedo, atmospheric

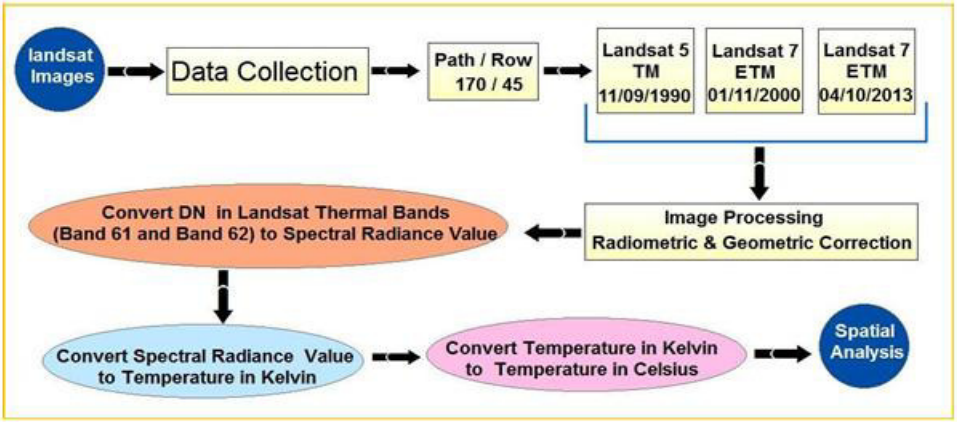

Figure 2: The major steps of study procedures

transmissivity, NDVI, LAI and surface emissivity (Liang et. al., 2003) developed a series of algorithms for calculating albedo from various satellite sensors and normalized by Smith (2010):

$$\alpha_{short} = \hat{} (0.356r_1 + \ddagger 0.130r_3 + \ddagger 0.373r_4 \ddagger + 0.085r_5 + \ddagger 0.072r_7 - 0.0018)/1.016$$

Where α_{short} is the weighted albedo at the top of atmosphere and r1, $2_{...n}$ are the reflectance values for each bands. The weighted albedo at the top of atmosphere, were calibrated with respect to atmospheric transmittance and the incoming shortwave radiation flux for all bands, that are reflected back to the sensor before reaching the surface (Waters et al., 2002; Opoku-Duah et al., 2008).

The surface albedo (αs) is calculated as follow:

$$\alpha s = (\alpha t - \alpha a)/ \tau 2bb$$

where αt=at-satellite broadband bidirectional albedo; αa = atmospheric (path) induced albedo; and τ^2_{bb} two-way broad-band atmospheric transmittance that assumes equal transmissivity for incoming and outgoing radiation (Tasumi et al., 2008). αa value is ranged from 0,025 to 0.04 (Fairs and Reddy, 2010).

$$\tau_{sw} = 0.75 + 2x10^{-5} x\ z$$

Where ^{sw}: is the atmospheric transmissivity and z is the elevation in meters of weather station above sea level.

The Normalized Difference Vegetation Index (NDVI), and Leaf Area Index (LAI), are calculated from visible and near infrared bands of ETM+ imagery as follows: (Waters et al., 2002; Lillesand et al., 2014):

NDVI= (IR-R)/(IR+R) = (band4-band3)/(band4+band3)

To compute the Leaf Area Index (LAI), soil adjusted vegetation index (SAVI) is calculate first. Soil adjusted vegetation index is appropriate for regions with low vegetation cover and consequently higher percentage of soil reflectance (Jenerette et al., 2007):

SVAI= (1+L) x (band 4- band 3)/ (L + band 4+ band 3)

Where: L is a constant; its value depends on the area properties (properties (L= +/- 0.5).
The Leaf Area Index (LAI) is calculated from the following empirical equation.

LAI= - Ln ((0.69-SAVI)/0.59)/0.91

The surface emissivity (ε) is a factor that describes how efficiently an object radiates energy compared to a black body (Lillesand et al., 2014) and is estimated from NDVI and LAI and used to calculate the land Surface Temperature (LST) or Sea Surface Temperature (SST) values (Opoku and Duah, (2008) and Bastiaanssene et. al. (1998);

$$\varepsilon = 1.009 + 0.047 \times \ln(NDVI)$$ Or

$$\varepsilon = 0.97 + 0.003 \times LAI$$,

for $LAI < 3.0$, while for area with NDVI < 0 and Surface albedo < 0.047 ; the emissivity equal to 0.99 (Waters et. Al. 2002). The land or sea surface temperature (T_s) will be calculated from the following equation: (Weng et.al. 2004 and 2006).

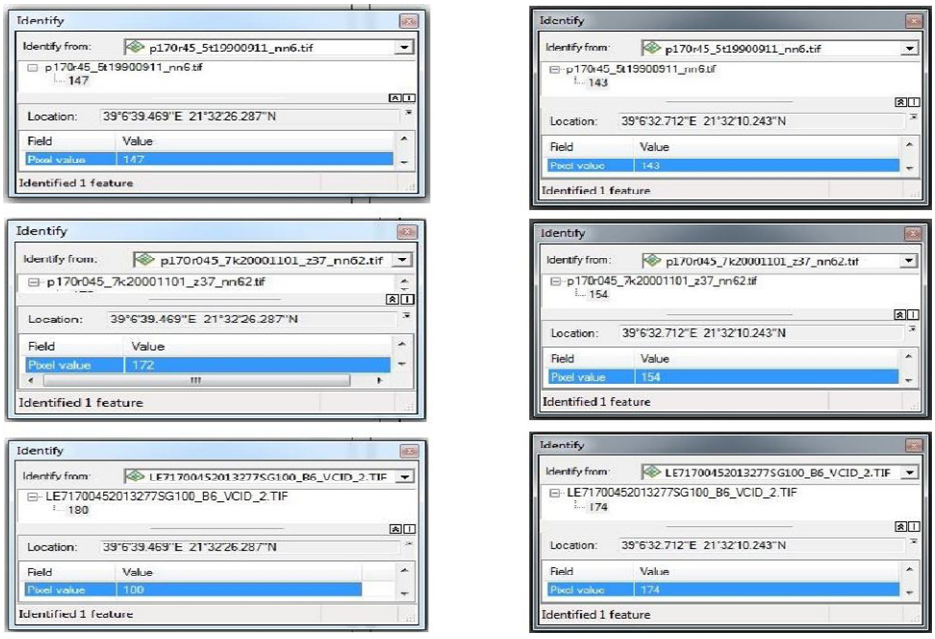

Figure 3: Geographic coordinates & DN for two locations

$$T_s = T_b / 1+(\lambda \times T_b / \gamma) \times \ln \varepsilon$$

Where λ = the average of limiting wavelengths of band 6 of ETM+ (λ=11.5 μm) ;

$\gamma = h \times c / a$ (0.01438m.K);

$a = Boltsmann constant\ (1.38 \times 10^{-23}\ j.k)$;

h=Plank's constant ($6.626 \times 10^{-34}\ J.s$);

$c = velocity\ of\ light\ (2.998 \times 10^{8}\ m/s)$

Step.3. Conversion of Kelvin to Celsius (Murayama and Lwin, 2013).

T_S = T (Kelvin) -273 (4)

Application on Retrieve (SST)

To explain the method of detect (SST) and Comparison of results. A number of two locations were selected (Figure3) (using band 61, band 62) to obtain and retrieve (SST).
In (Figure.3) the geographic coordinates of location in left side have the same (Degrees Minutes Seconds) 39°6'39.469"E 21°32'26.287"N, and have different (DN) values in each year as follows:

In year 1990 (DN= 147 band 6), In year 2000 (DN= 172 band 62), In year 2013 (DN= 180 band 62).

Right side in (Figure.3) the geographic coordinates for location have the same (Degrees Minutes Seconds) (39°6'32.712"E 21°32'10.243"N, and have different (DN) values in each year 1990 (DN= 143 band6), 2000 (DN= 154 band62), 2013 (DN= 174 band62).

RESULTS AND DISCUSSION

Computing SST from satellite data

To calculate (SST) for landsat5- TM (1990):

Equation (1) was used to convert the (DN) values to spectral radiance (L) value . CV_R= (0.055158 * 147) + 1.237800
CV_R= 9.346026
Equation (3) was used to convert the spectral radiance (L) values to temperature in Kelvin.

T= 1260.56 / 1n (607.76 / 9.346026 + 1) T (in Kelvin) = 300.843

Equation 4 was used to convert temperature (in Kelvin) to temperature in Celsius. T (°c) = 300.843 – 273
T (°c) = 28°c

To calculate (SST) for landsat7- ETM (2000):

A. Equation 2 was used to convert the (DN) values to spectral radiance (L) value . L= ((12.65 - 3.200)/ (255-1))* (172-1) +3.200 L= 9.562

B. Equation 3 was used to convert the spectral radiance (L) value to temperature in Kelvin.

Table 5: Landsat 7 ETM Thermal Band Calibration Constants

Sensor	Constant	1- K1	Constant 2 - K2
	watts/(meter squared * ster * µm)		
Landsat 7	666.09		1282.71
Landsat 5	607.76		1260.56

Table 6: Retrieve (SST)

year	DN	spectral radiance (L)	(SST) in Kelvin	(SST°c)
1990	147	9.346	300.843	28
2000	172	9.562	301.255	28
2013	180	9.859	303.408	30

T= 1282.71/ 1n (666.09/ 9.562+1) T= 301.255

C. Equation 4 was used to convert temperature (in Kelvin) to temperature in Celsius. T (°c) = 301.255 – 273

T (°c) = 28°c

To calculate (SST) for landsat7- ETM (2013):

A. Equation 2 was used to convert the (DN) values to spectral radiance (L) values . L= ((12.65 - 3.200)/ (255-1))* (180-1) +3.200

L= 9.859

B. Equation 3 was used to convert the spectral radiance (L) value to temperature in Kelvin.

T= 1282.71/ 1n (666.09/ 9.859645669+1) T= 303.408

C. Equation 4 was used to convert temperature (in Kelvin) to temperature in Celsius.
T (°c) = 303.408– 273

T (°c) = 30°c

The results are shown in (table 6)

Satellite images analyses

The impact of industrial wastewater and cooling water injection Led to a noticeable increase of sea surface temperature (SST). The results of this study indicate thermal pollution evidence at the Industrial Coastal Areas of Jeddah City. Figure 6 shows Lndsat7-ETM / band combination of channels (7.4.2) to display (LC & LU) relevant to the study area, such as industrial coastal area, coast line, residential area, green area… and so on. Figure.7 shows Lndsat7-ETM band combination of channels (6.2.1) to display thermal pollution areas. Figure(8) shows thermal band (band 61 & band 62) to identify the pixel value (DN) of several locations that were selected to represent thermal pollutions areas, validated by field measurements. Figure (9) shows thermal pollution area (red color) during the study period (1990, 2000, and 2013), by Visual interpretation using software ArcGIS 10.0.

According to the steps, previously explained, SST values were calculated for a number of 10 geographic locations in each of the years (1990, 2000 and 2013) to conclude thermal pollution areas. Table (7) shows (SST) values in the (10) selected locations, where thermal pollution areas for each year (1990, 2000 and 2013) were defined. It can be noticed that there is a change in (SST) between 1990 and 2013, also no change is noticed in (SST) between 1990 and 2000. The highest (SST) value (33°C) is found in 2013, while it was (28°C) in years 1990 and 2000 at the same geographic location. The lowest (SST) value (29°C)

Figure 4: Lndsat7-ETM / band combination of channels (7.4.2)

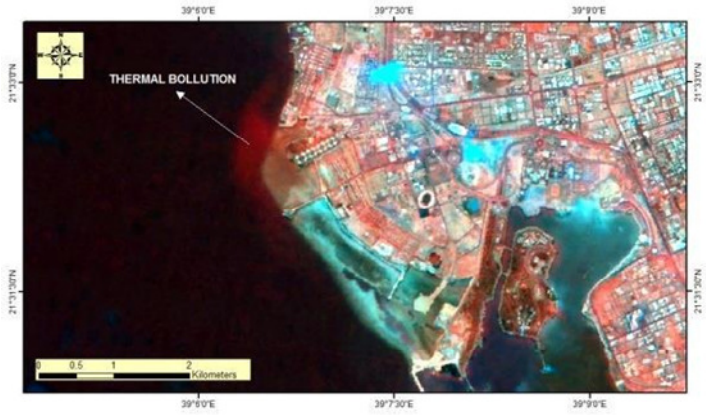

Figure 5: Lndsat7-ETM / band combination of channels (6.2.1)

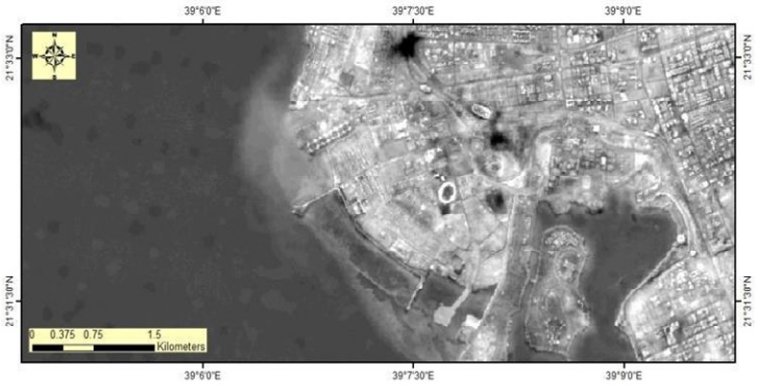

Figure 6: Lndsat7-ETM Thermal bands (band 61 & band 62)

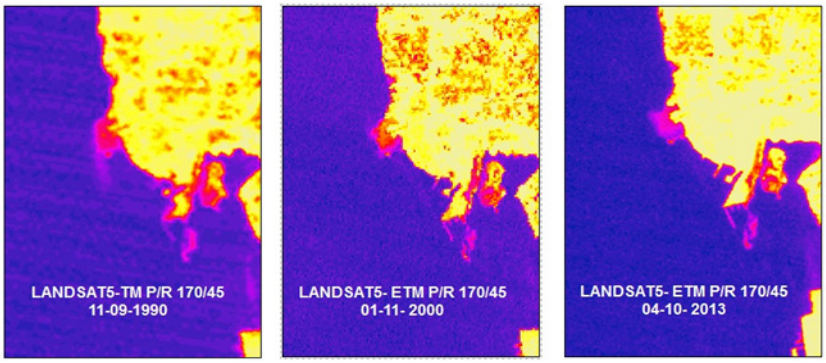

Figure 7: Thermal pollution area (red color) in each year

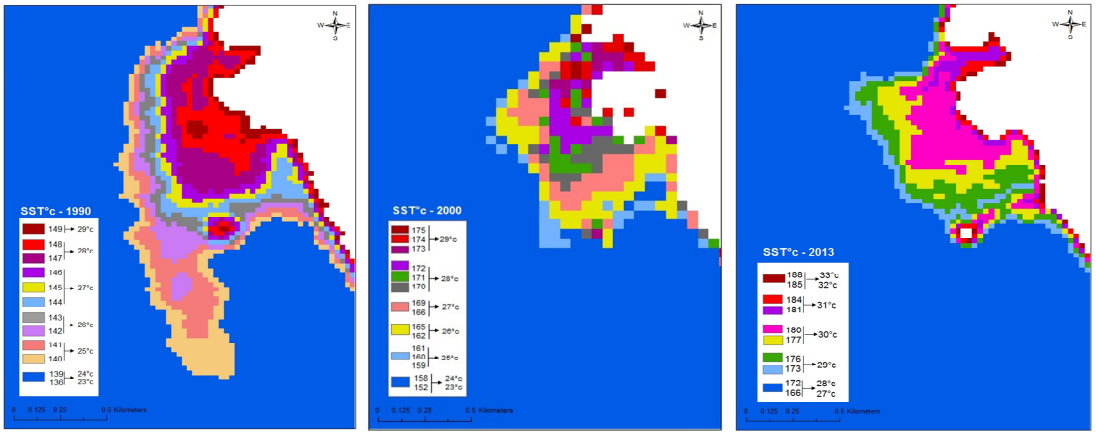

Figure 8: Distribution of (SST) in thermal pollution area

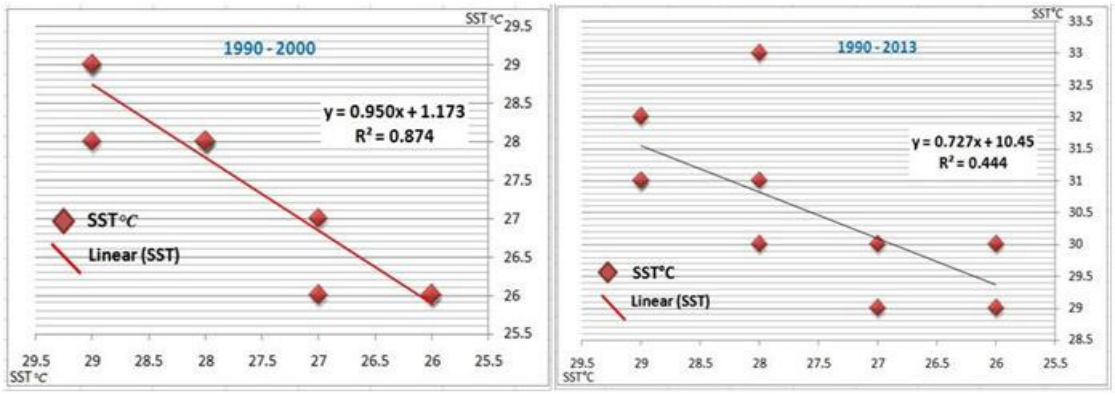

Figure 9: Correlation Coefficient between SST during 1990, 2000, 2013.

in 2013, while was (27°C & 26°C) in years 1990, 2000 at the same geographic location. Thus, average change rate in SST at thermal pollution areas during the period 2000 to 2013 equal to (18%) based on results of the following equation:

T (%) = (T2-T1)*100/ T1 [12]

Figure (8) shows (SST) distribution in coastal area of Jeddah city in September, October and November. Figure (9) shows the correlation between (SST) in (September 1990) and (November 2000). Relationship with (R= 0.935, R2 = 0.874). And shows the correlation between (SST) in (September 1990) and (October 2013). Relationship with (R= 0.667, R2 = 0.444). The distribution pattern of SST for

both data in (September 1990) and (November 2000) is similar largely, and the distribution pattern of SST for both data in (September 1990) and (October 2013) is relatively different.

Hazardous of thermal pollution

Thermal pollution is an act of altering the temperature of a natural water body, which may be a river, lake or oceanic environment. This condition chiefly arises from the waste heat generated by an industrial process such as certain power generation plants. Many aquatic organisms are very sensitive to small temperature changes of as little as one degree Celsius. The temperature changes not only alter metabolic rates, but also may affect cellular biology, including reduction of cell wall permeability, harming osmotic processes, in addition, to alteration of enzyme metabolism and coagulation of cell proteins, (Hogan, 2010). These stenothermic organisms can be killed by sudden temperature changes that are beyond the tolerance limits of their metabolic systems. Periodic heat treatments used to keep the cooling system clear of fouling organisms that clog the intake pipes can cause fish mortality (Pokale, 2012).

CONCLUSION

The obtained results draw the attention to the evidences of a thermal pollution in Jeddah City Coastal Areas due to industrial cooling water injection and the increase in (SST). It is expected that such SST rise have its impact on different aquatic and agro-environmental system.

REFERENCES

Aleem A (1990): Impact of human activity on marine habitats along the Red Sea coast of Saudi Arabia, Hydrobiologia, 208 (1990) 7-15.

Bastiaanssen W, Menenti M, Feddes R, Holtslag A (1998): A remote sensing surface energy balance algorithm for land (SEBAL). 1. Formulation, Journal of hydrology, 212 (1998) 198-212.

Carbonneau P, Piégay H (2012): Fluvial remote sensing for science and management, John Wiley and Sons, 2012.

Faris A, Reddy YS (2010): Estimation of urban heat island using Landsat ETM+ imagery at Chennai city—a case study, Int J Earth SciEng, 3 (2010) 332-340.

Hogan CM (2010):Water pollution, Encylopedia of earth topic. Washington, DC: Cleveland National Council on Science and Environment, (2010).

Irons J (2012): Landsat 7 science data user's handbook, in, Report 430-15-01-003-0.National Aeronautics and Space Administration [online]. Available from: http://landsathandbook. gsfc. nasa. gov/[Accessed 6 July 2012], 2011.

Jenerette GD, Harlan SL, Brazel A, Jones N, Larsen L, Stefanov WL (2007): Regional relationships between surface temperature, vegetation, and human settlement in a rapidly urbanizing ecosystem, Landscape Ecology, 22 (2007) 353-365.

Liang S, CJ (2003): Shuey, A.L. Russ, H. Fang, M. Chen, C.L. Walthall, C.S. Daughtry, R. Hunt, Narrowband to broadband conversions of land surface albedo: II. Validation, Remote Sensing of Environment, 84 (2003) 25-41.

Lillesand T, Kiefer RW, Chipman J (2014): Remote sensing and image interpretation, John Wiley and Sons, 2014.

Mitasova H, Neteler M (2004): GRASS as open source free software GIS: accomplishments and perspectives, Transactions in GIS, 8 (2004) 145-154.

Murayama Y, Lwin K (2013): Estimation of Landsat TM surface temperature using ERDAS Imagine Spatial Modeler. University of Tsukuba, Ibaraki, Japan, 2010, in, 2013.

Opoku-Duah S, Donoghue D, Burt T (2008): Intercomparison of evapotranspiration over the Savannah Volta Basin in West Africa using remote sensing data, Sensors, 8 (2008) 2736-2761.

Pokale W (2012): Effects of thermal power plant on environment, Scientifics Reviews and Chemical Communications, 2 (2012) 212-215.

Prakash A (2000): Thermal remote sensing: concepts, issues and applications, International Archives of Photogrammetry and Remote Sensing, 33 (2000) 239-243.

Quattrochi DA, Luvall JC (1999): Thermal infrared remote sensing for analysis of landscape ecological processes: methods and applications, Landscape ecology, 14 (1999) 577-598.

Sarkar A, Gaitonde DC, Sarkar A, Vashistha D, D'Silva C, Dalal S (2008): Evaluation of impairment of DNA integrity in marine gastropods (Croniacontracta) as a biomarker of genotoxic contaminants in coastal water around Goa, West coast of India, Ecotoxicology and environmental safety, 71 (2008) 473-482.

Schott J (1982): AN APPLICATION OF HEAT-CAPACITY MAPPING MISSION DATA-THERMAL BAR STUDIES OF LAKE-ONTARIO, Journal of Applied Photographic Engineering, 8 (1982) 117-120.

Simonovic SP, Eng P, (2002): Role of remote sensing in disaster management, (2002).

Smith R (2010): The heat budget of the earth's surface deduced from space" available on http://www. yale. edu/ceo, Documentation/ceo_faq. html, (2010).

Stefouli M, Vasileiou E, Charou E, Stathopoulos NPA, GP (2013): REMOTE SENSING TECHNIQUES AS A TOOL FOR DETECTING WATER OUTFLOWS. THE CASE STUDY OF CEPHALONIA ISLAND in: Bulletin of the Geological Society of Greece (Ed.) Proceedings of the 13th International Congress, Bulletin of the G.S.G., Chania, Crete, Greece, 2013, pp. 1519-1528.

Tarantino E, Aielo ACM (2011): THE CONTRIBUTE OF THERMAL INFORMATION TO MAP VULNERABILITY OF INDUSTRIAL COASTAL AREAS in: A.R.o.b.o.t.F.C.o. Cartography. (Ed.) Proceedings of the 25th International Cartographic Conference, Paris, France,, 2011.

Tasumi M, Allen RG, Trezza R (2008): At-surface reflectance and albedo from satellite for operational calculation of land surface energy balance, Journal of hydrologic engineering, 13 (2008) 51-63.

UA PERSGA (1997): Assessment of Land-based Sources and Activities Affecting the Marine Environment in the Red Sea and Gulf of Aden, , UNEP Regional Seas Reports & Studies, 166 (1997) 67.

UNESCO (2007): REMOTE SENSING APPLICATIONS to GROUNDWATER, (2007).

Waters R, Allen R, Bastiaanssen W, Tasumi M, Trezza R, SEBAL (2002): Surface Energy Balance Algorithms for Land. Idaho Implementation.Advanced Training and Users Manual, Idaho, USA, (2002).

Weng Q, Lu D, Schubring J (2004): Estimation of land surface temperature–vegetation abundance relationship for urban heat island studies, Remote sensing of Environment, 89 (2004) 467-483.

Weng Q, Yang S (2006): Urban air pollution patterns, land use, and thermal landscape: an examination of the linkage using GIS, Environmental monitoring and assessment, 117 (2006) 463-489.

Wise GEEK NP (2014): What Are the Most Common Causes of Pollution, in: Wise GEEK (Ed.), Conjecture Corporation, 2014.

Xing Q, C.-q. Chen, Shi P (2006): Method of integrating Landsat-5 and Landsat-7 data to retrieve sea surface temperature in coastal waters on the basis of local empirical algorithm, Ocean Science Journal, 41 (2006) 97-104.